SD2225 ground vehicle dynamics project, Final report: modeling and simulation of a volvo s90 with adams car and the bicycle model

Group 14: Carlo Vittorio Colucci, Simon Loriot
& Jad El Madani

May 2025

Contents

1 Introduction

The aim of this report is to model a Volvo S90, using on the one hand the software Adams Car and on the other hand an improved bicycle model on Matlab coupled with data from field testing of the vehicle. The methodology followed on Adams is explained, and the main subsystems are tested. Simple analytical calculations are performed to validate the order of magnitude of the results from the simulations. As far the Matlab model goes, the brush model will be used. A comparison for standard maneuvres will be made after the full vehicle assembly on Adams. Finally a parameter study will be showcased and the sources of error in the project highlighted.

2 Modeling of the Volvo S90 with Adams Car

2.1 Key steps followed to create an Adams car simulation

The main steps to create an Adams car simulation are the following:

1- Defining the hardpoints to set the location of the components and the local reference frames

2- Creating general parts, arms, links and mounts

3- Assigning a geometry for 3D animations

4- Creating joints and bushings to determine the relative motion of the parts

5- Creating forces (springs, dampers...)

6- Finalizing the template

7- Creating subsystems based on the templates

8- Creating an assembly based on the subsystems

9- Choosing input parameters for the simulation (number of steps, desired displacement/roll/steering angle)

2.2 The front suspension and the steering system

The first subsystem that was created is the front suspension. It is a double wishbone suspension, connected to an anti-roll bar. The steps from section 2.1 were followed. For comparison, a sketch is given below next to the Adams Car assembly.

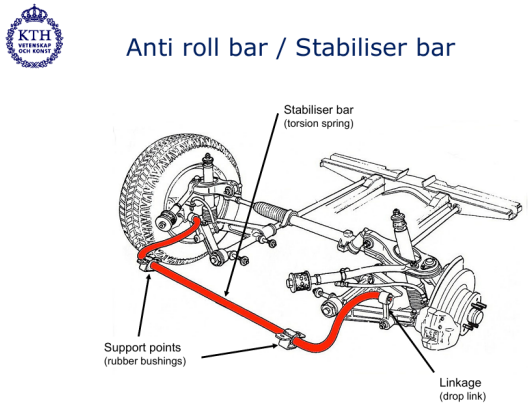

(a) Sketch of a double wishbone with anti-roll bar from SD2222 vehicle components

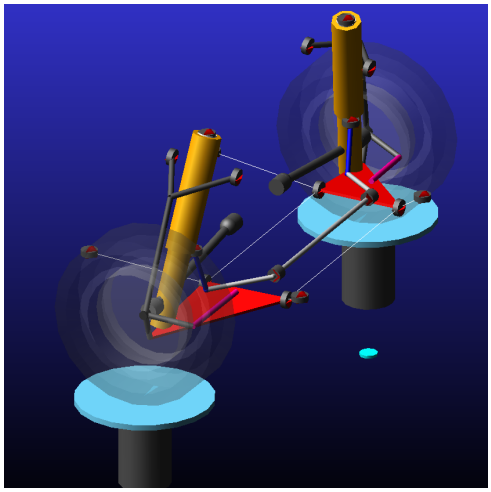

(b) Double wishbone front suspension modeled on Adams

2.2.1 Analytical calculation without the anti-roll bar and comparison with Adams

A simple 2D theoretical model was built for the front double wishbone without an anti-roll bar in order to have comparison material with simulation results. A sketch of the model is given below:

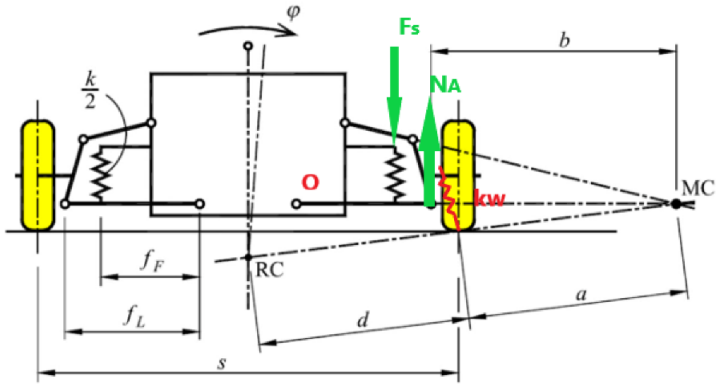

Figure 2: Simplified double wishbone model [SD2225 Ground Vehicle Dynamics]

The geometrical parameters are the following: f_F is the distance between the inner attachment point of the lower control arm and the spring's attachment point. f_L is the length of the lower control arm. b is the distance between the lower control arm's outer attachment point and the instantaneous center of rotation. a is the distance between the center of the contact patch and the instantaneous center of rotation. Rigorously speaking, a and b are functions of time but for simplicity they will be considered constant here and hence computed in the initial configuration of the system.

First, relations need to be found between the relevant displacements of the problem. Let δ_s the displacement of the spring, δ_A the displacement of the outer attachment point of the lca, δ_W the displacement of the wheel. Using small displacements assumption, the following figure depicts the displacements occurring in the system:

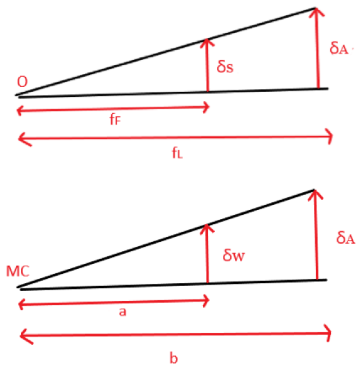

Figure 3: Displacements, double wishbone suspension

From the above figure:

$\boxed{\frac{\delta_s}{f_F} = \frac{\delta_A}{f_L}}$ **(1)**

$\boxed{\frac{\delta_W}{a} = \frac{\delta_A}{b}}$ **(2)**

A moment equilibrium about O yields:

$F_s f_F = N_A f_L$

i.e $k_s \delta_s f_F = k_A \delta_A f_L$

Given **(1)**:

$\boxed{k_A = k_s(\frac{f_F}{f_L})^2}$ **(3)**

A moment equilibrium about MC yields:

$k_W \delta_W a = k_A \delta_A b$

Given **(2)** and **(3)**:

$\boxed{k_W = k_s(\frac{b}{a})^2(\frac{f_F}{f_L})^2}$ **(4)**

The total load at the wheel can then be defined as:

$\boxed{F_W = F_0 + k_W \delta_W}$ **(5)** F_0 a static load

A test was then performed for a displacement between $+-100\ mm$. The results were exported from Adams to Matlab. The geometrical parameters were assessed using the projection of the hard-points on the (y, z) plane. The static load of the theoretical model was adjusted according to Adams test-rig.

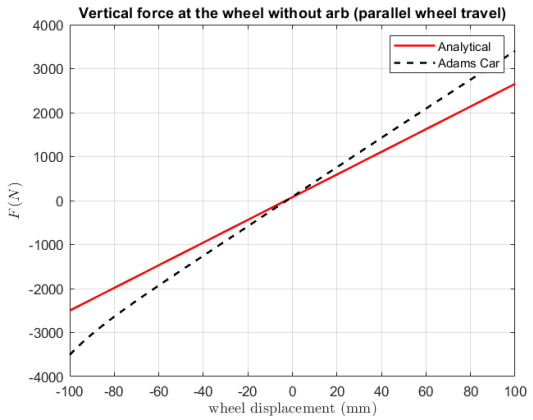

(a) Vertical force vs wheel travel adams vs theory (parallel travel)

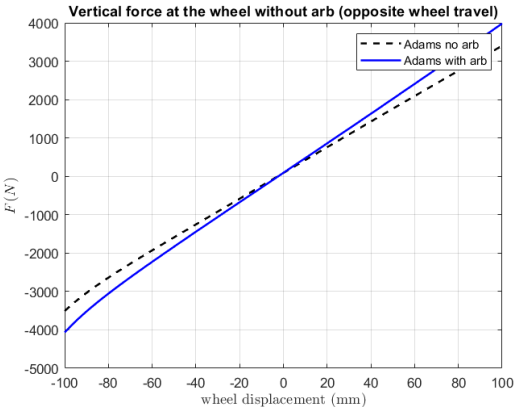

(b) Vertical force vs wheel travel adams with and without anti-roll bar (opposite travel)

The results of the parallel wheel travel (theory vs adams, left plot) show that $k_{W_{Adams}} \approx 33.3$ N/mm, $k_{W_{theory}} \approx 25.77$ N/mm, which is of the same order of magnitude but still presents a considerable discrepancy, probably due to the numerous approximations that were made in the model (3D geometry to 2D, b and a assumed constant...). Besides, with an opposite wheel travel simulation, the additional stiffness from the anti-roll bar is observed ($k_{W_{new}} = 39.13$ N/mm).

2.2.2 Steering system

The next step was to add the steering system to the front suspension. The steering is maneuvered by a rack and pinion mechanism. A reduction ratio (distance covered by the rack for one rotation of the pinion) is used to determine the steering range where the steering gear ratio lies.

(a) Rack and pinion steering system from SD2222 vehicle components

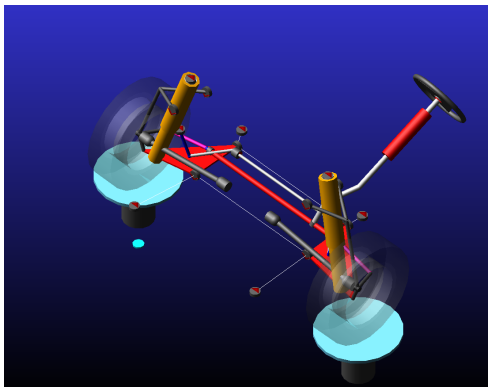

(b) Rack and pinion steering system modeled on adams

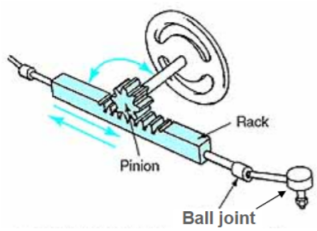

Figure 6: Focus on the rack and pinion [from SD2222]

A simulation was performed for an input steering wheel angle between +-80°. The steering angle at the wheel was plotted against the steering wheel input. Furthermore, the steering gear ratio $i_s = \frac{\delta_{SW}}{\delta_W}$ is computed and plotted. The reduction ratio is adjusted to 0.09 by trial and error in order to get a steering gear ratio that stays as close as possible to the target given in the vehicle data sheet (16.3).

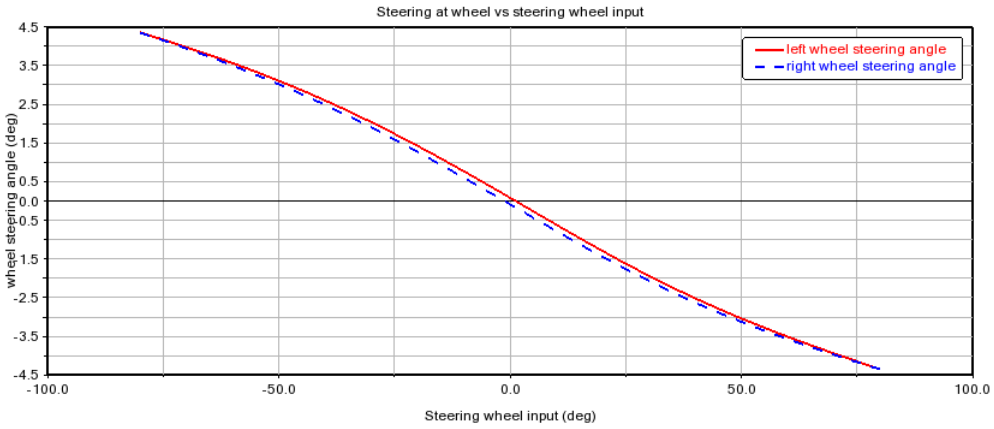

Figure 7: steering angle vs steering wheel input

The first result is consistent: the greater the steering input the greater the steering angle at the wheel (in absolute value). There is a slight difference between left and right wheels.

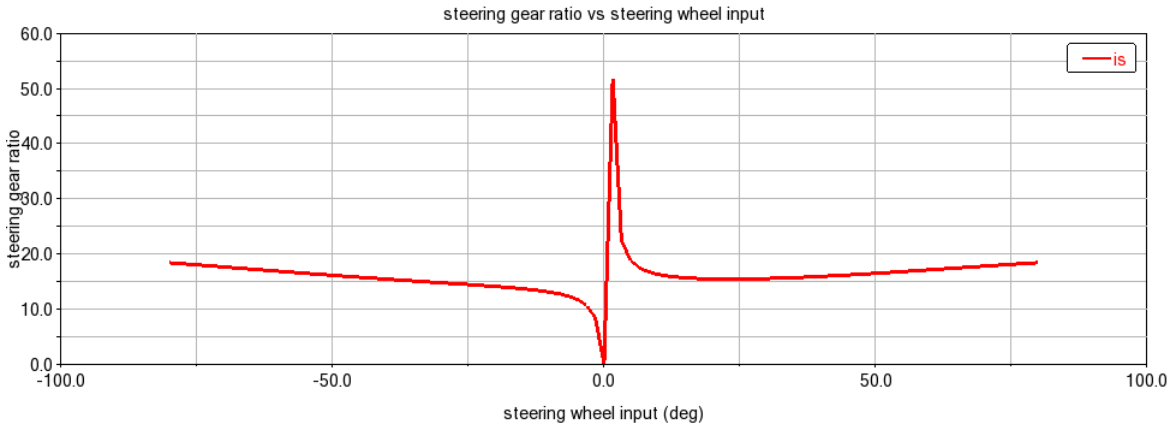

Figure 8: steering gear ratio

Except the singularity at 0 that is present just due to the way the steering gear ratio was computed, the steering stays relatively close to 15 which corresponds to the order of magnitude of 16.3.

2.3 The rear suspension

The design phase followed for the rear suspension subsystem is the same as the one introduced in Section 2.1.
One key step of the design is the implementation of the bushings in the model; their correct orientation is crucial to successfully run a model simulation and to retrieve accurate results. The main concept behind their orientation is that the major movements of the components, linked to the bushing, lay on the bushing xy plane of construction. A graphical representation of how the bushings have been oriented is shown below:

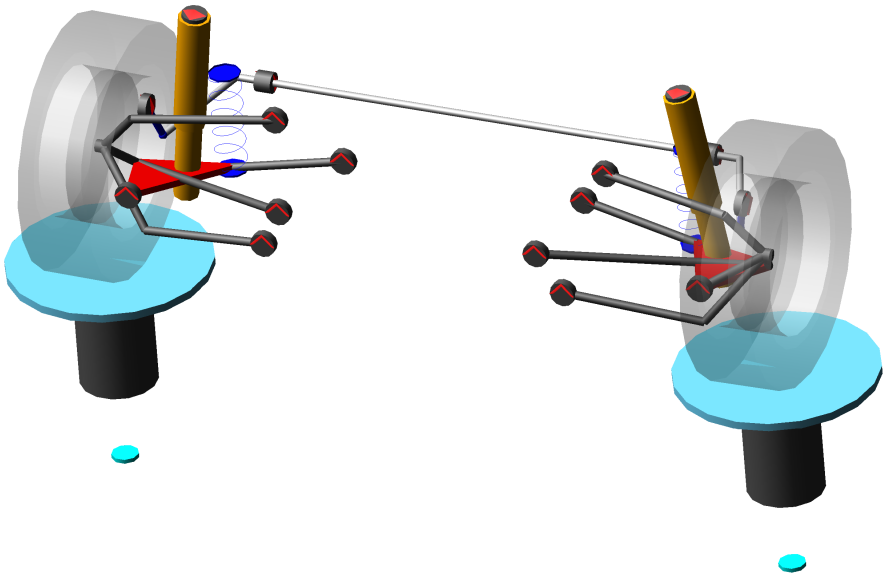

Figure 9: Rear suspension subsystem

Concerning the bushing positioned on the strut, to correctly and easily position it, a construction frame is defined. The idea is to align the frame z axis to the damper stem axis, since the bushing is meant to host the relative movement of the damper with respect to the strut:

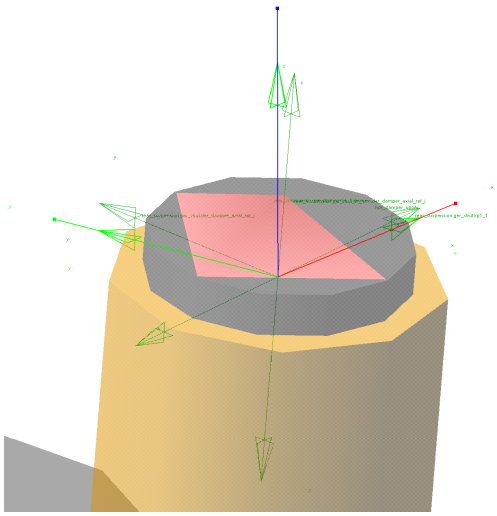

Figure 10: Focus on the strut bushing

During this design step, having a clear understanding of how the Euler angles work can be helpful to quickly orient the construction frames or specific elements themselves in the space.

Two different simulations are undertaken for the rear suspension subsystem:

- Parallel wheel travel: bound $= 80mm$, rebound $= -80mm$;
- Opposite wheel travel: bound $= 80mm$, rebound $= -80mm$.

The resulting vertical force trend at tire level for both the simulations is shown:

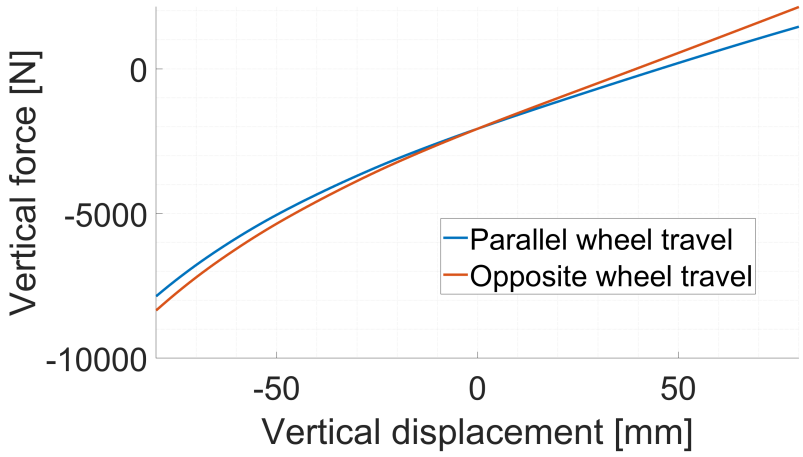

Figure 11: Parallel and opposite wheel travel simulation

It is interesting to compare the results retrieved by simulation, with the ones that can be retrieved by an analytical approach. To do so, it is necessary to understand what is the relation between the wheel travel and the vertical force production.
In the case of parallel wheel travel, it's possible to retrieve a relation between the suspension stiffness and an equivalent stiffness at the wheel level, as explained in Section 2.2.1:

$$K_w = K \cdot \left(\frac{f_F}{f_L}\right)^2 \cdot \left(\frac{b}{a}\right)^2 \tag{1}$$

Thus, the vertical force is directly computed:

$$F_z = K_w \cdot z + F_{z,0} \tag{2}$$

where $F_{z,0} = -2071.97N$ is the static vertical load.
In this particular situation, the effect of the anti-roll bar is negligible.
It is important to highlight that, although the rear suspension is a multi-link, its rolling stiffness characteristic is still defined in the same way as done for the double wishbone.

In the case of opposite wheel travel, the wheel displacement is strictly related to the vehicle roll angle. Then, exploiting the axle roll stiffness, the resulting moment is calculated:

$$C_r = C_{spring} + C_{arb} = 2 \cdot \left(\frac{b \cdot d \cdot f_F}{a \cdot f_L}\right)^2 \cdot K_R + C_{arb} \tag{3}$$

$$M_\phi = C_r \cdot \phi \tag{4}$$

Then, by a simple moment equilibrium balance, the vertical force at wheel level is computed:

$$F_z = M_\phi / t_w + F_{z,0} \tag{5}$$

In both these study cases, the lengths a, b, d, f_F and f_L are computed by the aid of the Adams hard-point positioning.

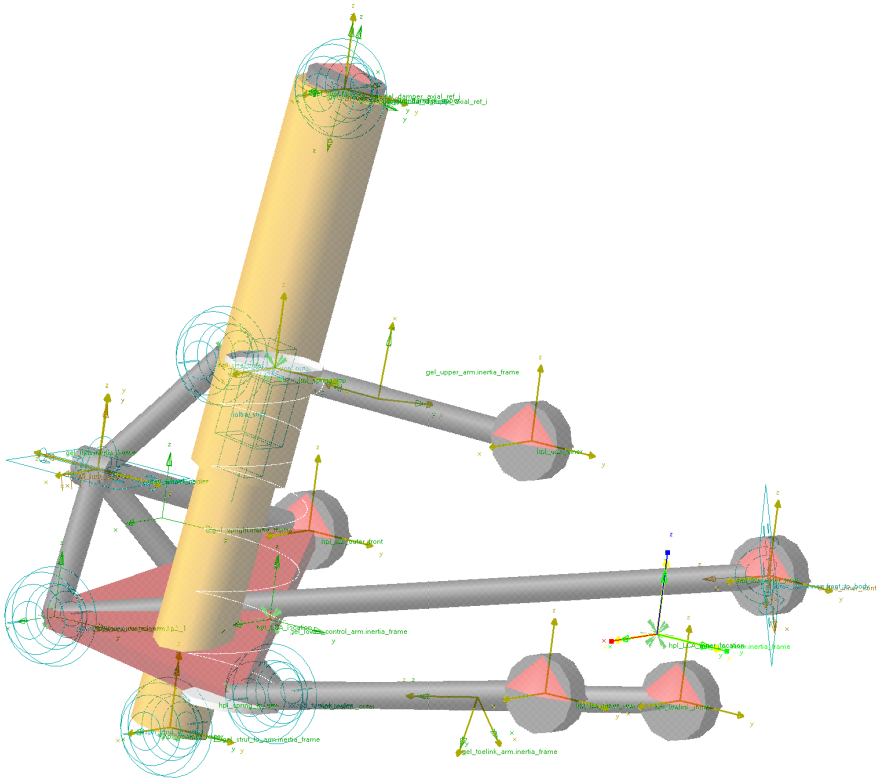

Figure 12: LCA inner location

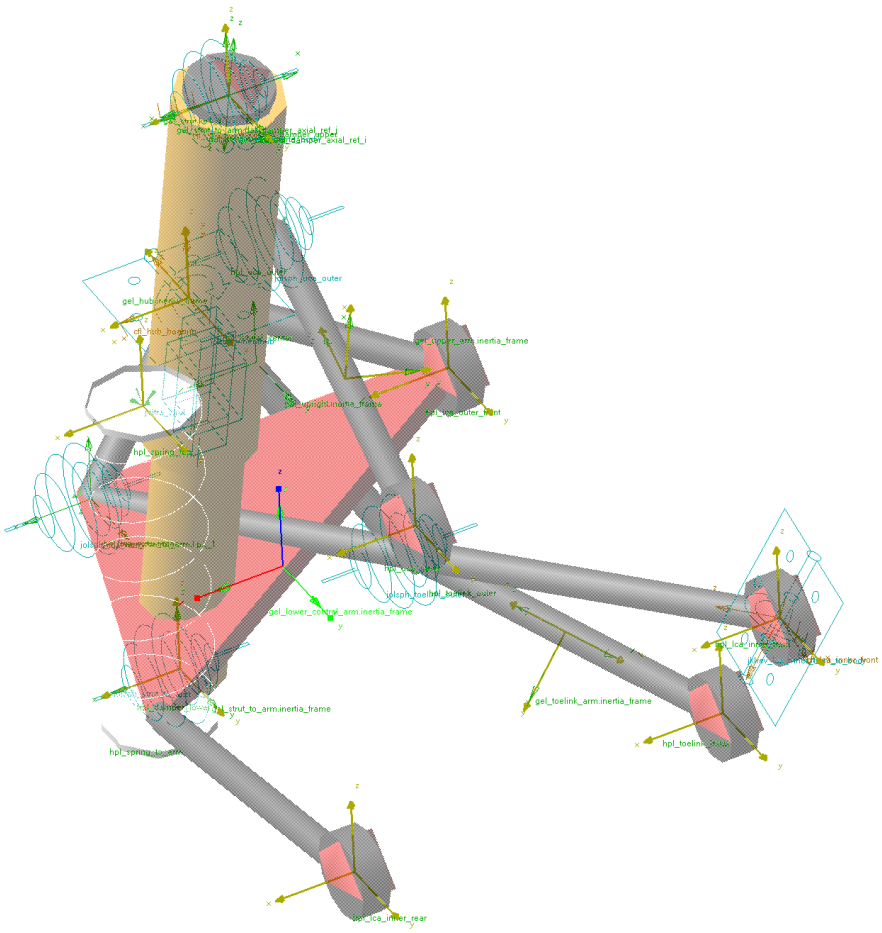

Figure 13: LCA outer location

Of course, during the wheel displacement, these values change, slightly varying the tire equivalent stiffness K_w as well as the axle rolling stiffness C_r but, as an assumption, they can be considered to be constant.
To evaluate these lengths it is necessary to locate some relevant hard points:

Point	y coordinate	z coordinate
UCA outer	-728	461
UCA inner	-406	470
LCA outer	-621.9	287.4
LCA inner	-305.5	339
Spring LCA attachment	-571	249
Contact patch	-814	0

Table 1: Rear suspension hard points

Then, defining the intersection of two lines in the 2D coordinate system passing through the UCA points and the LCA ones respectively, the IC (instant center) of rotation position is calculated:

$$\frac{z - UI_z}{UO_z - UI_z} = \frac{y - UI_y}{UO_y - UI_y}$$

$$\frac{z - LI_z}{LO_z - LI_z} = \frac{y - LI_y}{LO_y - LI_y}$$

$$\begin{cases} z = 0.028 \cdot y + 481.348 \\ z = 0.163 \cdot y + 388.822 \end{cases}$$

$$IC : [685.4;\ 500.5]$$

Eventually, intersecting the line connecting the IC to the contact patch with the vehicle symmetry line, the RC (roll center) position is calculated:

$$\frac{z - CP_z}{IC_z - CP_z} = \frac{y - CP_y}{IC_y - CP_y}$$

$$\begin{cases} z = 0.334 \cdot y + 271.739 \\ y = 0 \end{cases}$$

$$RC : [0;\ 271.7]$$

Now that the position of all the relevant points is defined, all the lengths can be calculated:

$$a = \sqrt{(IC_y - CP_y)^2 + (IC_z - CP_z)^2} = 1580.7mm$$

$$b = \sqrt{(IC_y - LO_y)^2 + (IC_z - LO_z)^2} = 1324.6mm$$

$$d = \sqrt{(CP_y - RC_y)^2 + (CP_z - RC_z)^2} = 858.1mm$$

$$f_F = |SLA_y - LI_y| = 265.5mm$$

$$f_L = |LO_y - LI_y| = 316.4mm$$

In order to evaluate the roll angle, it is reasonably assumed that it is a function of the vertical wheel displacement, according to the following equation:

$$\phi = \frac{z}{t_w/2} \tag{6}$$

Using this equation along with Equations 3, 4, 5, one comes up with the final analytical equation of the vertical force as a function of the wheel vertical displacement:

$$F_z = \frac{2 \cdot C_r \cdot z}{t_w^2} + F_{z,0} = \frac{2 \cdot \left[2 \cdot \left(\frac{b \cdot d \cdot f_F}{a \cdot f_L}\right)^2 \cdot K_R + C_{arb}\right] \cdot z}{t_w^2} + F_{z,0} \tag{7}$$

where:

$$K_R = 80kN/m, \quad C_{arb} = 0.57kN \cdot m/rad, \quad t_w = 1.626m$$

Now that all the data are available, a comparison of the vertical force retrieved by Adams, with the trend retrieved by analytical calculations is retrieved (the same data set of wheel vertical displacement is considered):

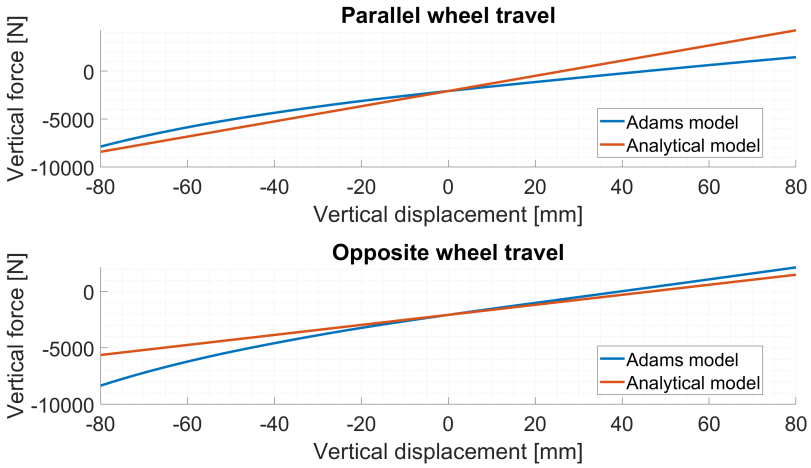

Figure 14: Comparison between Adams and analytical model

It is visible how the prediction made by the analytical model fits pretty well the accurate results computed by Adams, confirming the adopted model validity.

2.4 Full vehicle assembly

Templates were created and adjusted for the wheels, the powertrain, the brakes and the chassis. Subsystems were then obtained from the templates and assembled with the suspensions. The result is given below:

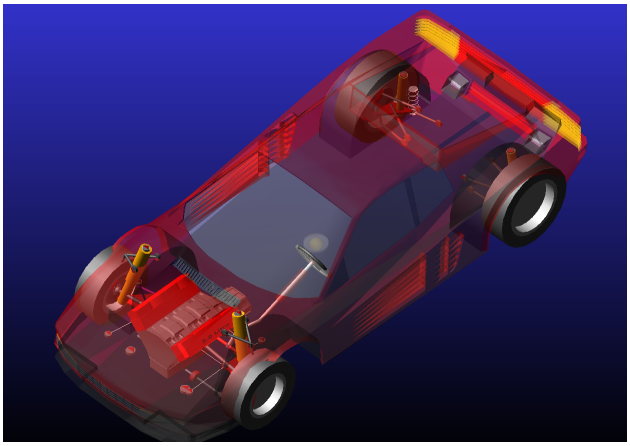

Figure 15: Full vehicle assembly on Adams Car

The obtained assembly ran without errors for a single lane change simulation, but it presented issues: the driveshaft constantly fell to the ground which consequently corrupted the results. Hence, given the time left for the project, the provided database was used instead. Below an example of a standard single lane change using the provided database, to show that it functions properly:

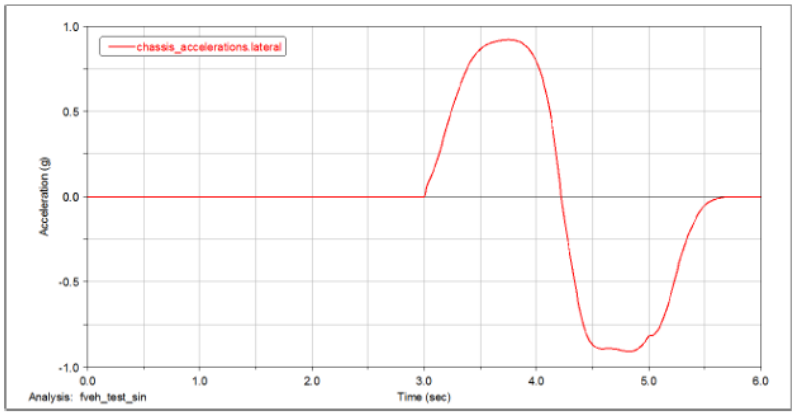

(a) Reference from adams user guide

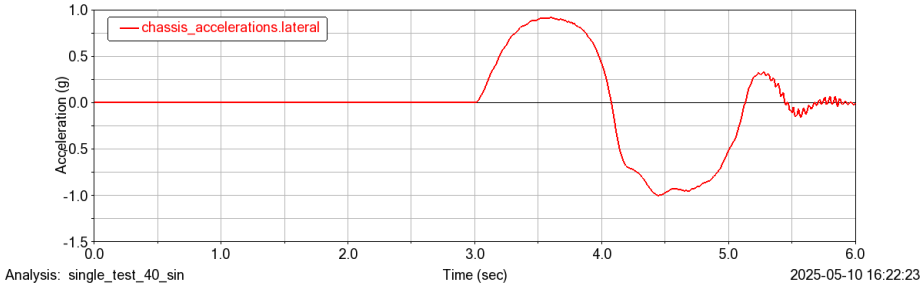

(b) Result from the provided database

Figure 16: lateral acceleration single lane change

2.5 Difficulties encountered during the modeling

During the modeling phase on Adams, multiple difficulties were faced, mainly for the front suspension assembly and the full vehicle assembly.

2.5.1 Front suspension

At the beginning of the project, the front suspension simulations crashed for large inputs: more than 35 mm displacement or more than 80° steering input. The solution that was found towards the end was to change a coordinate reference in the joint tripot to differential from hpl_... to hpr_. This was found out by reverse engineering the provided templates: a comparison was made, differences were identified and the working model was altered till it broke, which led to the "key" modification.

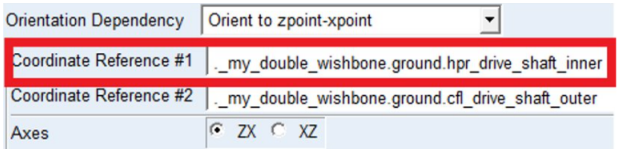

Figure 17: Front suspension: coordinate reference adjustment

2.5.2 Full vehicle assembly

As far as the full vehicle assembly goes, the issues came from the communicators, which ensure that all subsystems exchange data properly. At the beginning, all simulations failed because of large displacements (10^9...). The issue was that some input communicators missed outputs and were by default linked to the ground. It can be highlighted that the output of one subsystem can be in an other subsystem.

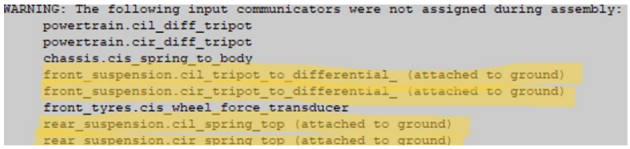

Figure 18: Full vehicle assembly: communicators issue

Nevertheless, as mentioned in the full vehicle assembly section, there was still an issue with the driveshaft that could not be solved. Probably a communicator that was not correctly defined.

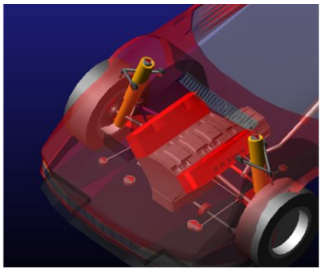

(a) Initial position of the drive shaft

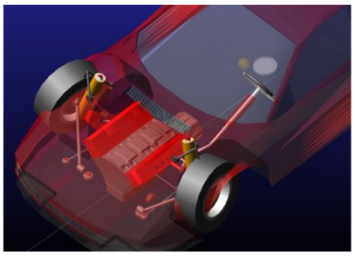

(b) Detachment from the engine

Figure 19: Full vehicle assembly issue

3 Modeling of the Volvo S90 with Matlab

Another model for the car was created using MATLAB in order to compare the results with ADAMS and the testing. The bicycle model was chosen for its simplicity. The assumption is that the car behaves like a bicycle with the effect of the tires in the same axle being combined in one tire. A sketch of the bicycle model is represented in figure 20.

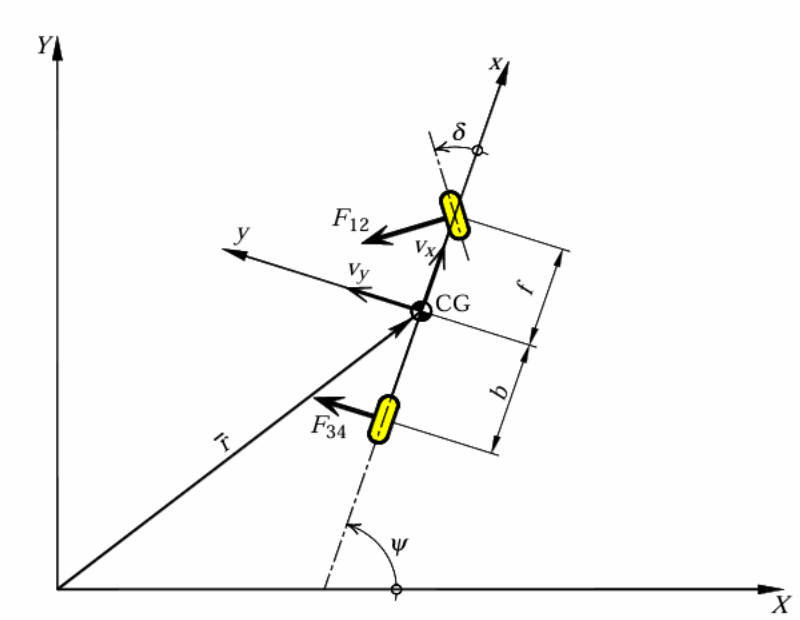

Figure 20: Bicycle Model [from SD2225]

The equations of the model can be derived using Newton's law of motion :

$$m(\dot{v_y} + \dot{\psi} v_x) = F_{34} + F_{12} \ (1)$$

$$J_z \ddot{\psi} = f F_{12} - b F_{34} \ (2)$$

To complete the model, the lateral forces F_{12} and F_{34} should be expressed. The choice of a tire model will have a critical influence on the behavior of the car.

The model being complete, the equations can be numerically integrated using Euler forward numerical scheme with a fixed time step. The control input is the steering angle at the wheel (δ) and the longitudinal speed (v_x).

3.1 Linear model

A linear model was implemented into the matlab code. It is the simplest tire model, where the lateral force F_i is directly proportional to the slip angle α_i. Therefore :

$$F_i = -C_i \alpha_i \ (3)$$

Where α_i is obtained using the geometry of the car :

$$\alpha_{12} = \frac{v_y + \dot{\psi} f}{v_x} - \delta \ (4)$$

$$\alpha_{34} = \frac{v_y - \dot{\psi} b}{v_x} \quad (4)$$

The coefficient C_i is called the cornering stiffness and is a tire parameter.

This model works under the assumption of a small slip angle ($\alpha_i << 1$). At higher slip angles, the model becomes less accurate.

3.2 Brush model

Another model was also implemented to obtain more complex tire behavior at higher slip angles. The brush model was chosen because it can handle the saturation of the tires.

The main assumption of this model is that the displacement of the bristles is linear along the direction of the tire. At high slip angle, a part of the tire will start to slide, saturating the lateral forces. The total lateral force on the tire is represented in figure 21.

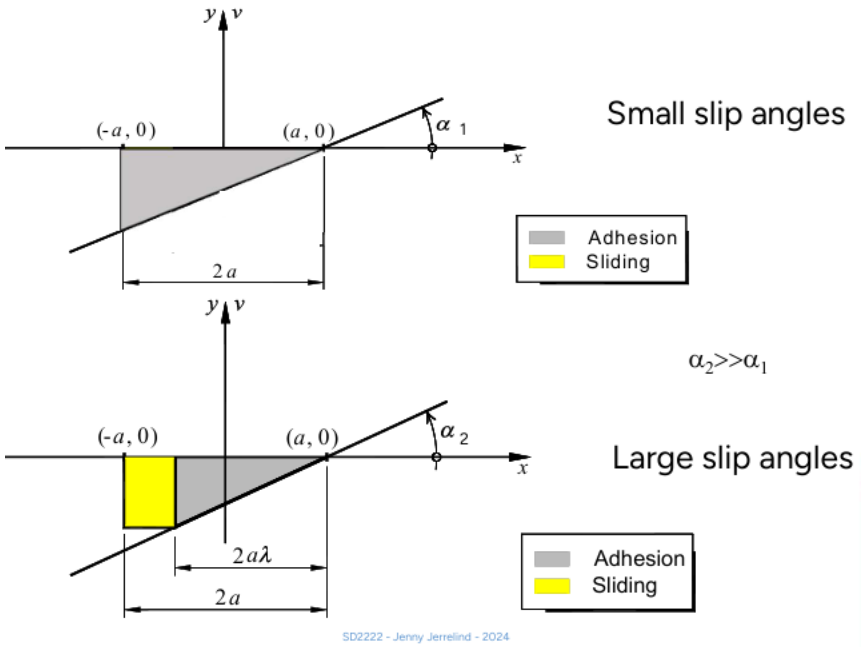

Figure 21: Brush model [from SD2222 Vehicle components]

The formula for the lateral force can be derived :

$$F_i = -C_i tan(\alpha_i) f(\lambda) \quad (5)$$

$$\lambda = \frac{F_z \mu}{2C_i |tan(\alpha_i)|}$$

$$f(\lambda) = \begin{cases} \lambda(2-\lambda) & \text{if } \lambda \leq 1 \\ 1 & \text{if } \lambda > 1 \end{cases}$$

For small slip angles, we have $tan(\alpha) \approx \alpha$ and the brush model is linear. For higher slip angles ($\alpha \approx 90$), we have $F_y \approx -F_z\mu \cdot sign(\alpha)$, the tire is saturated. The lateral force against slip angle is represented figure 22

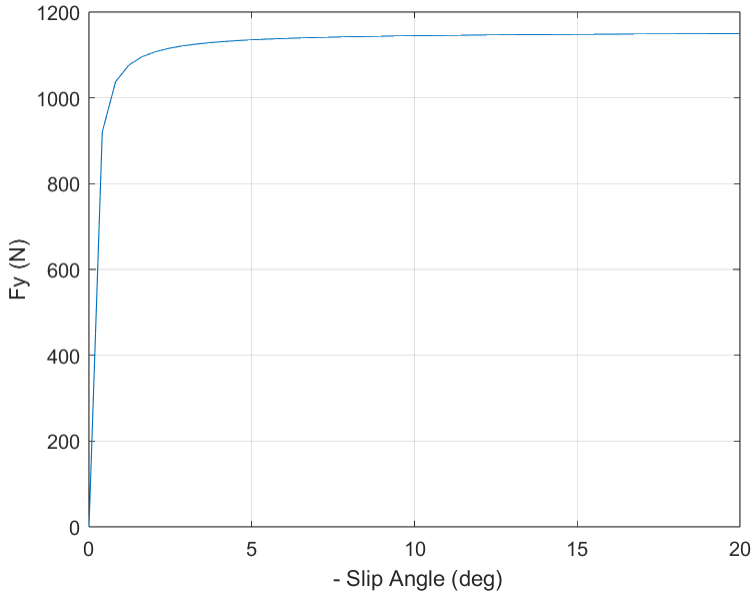

Figure 22: Lateral Force against slip angle

We can notice that the tire force depend on the vertical force F_z. Without any longitudinal acceleration, we have $F_{z12} = \frac{b}{L}mg$ and $F_{z34} = \frac{f}{L}mg$. A possible improvement of the model would be to implement the longitudinal load transfer into the model.

3.3 Comparison between the models

To compare the different tire models, a test was created with a fixed longitudinal speed $v_x = 50km/h$ and a fixed steering angle δ. Both models will be tested with the same parameters : $C_{12} = 90kN/rad$, $C_{34} = 100kN/rad$ and $\mu = 1.2$.

A first test was concluded with a steering angle at the steering wheel of $\delta_{sw} = 40°$. In both models, the car describes a circle of approximately $80m$ of radius. No significant differences were observed between the two models. The respective trajectories are represented by figure 23

Figure 23: Trajectory for $\delta_{sw} = 40$

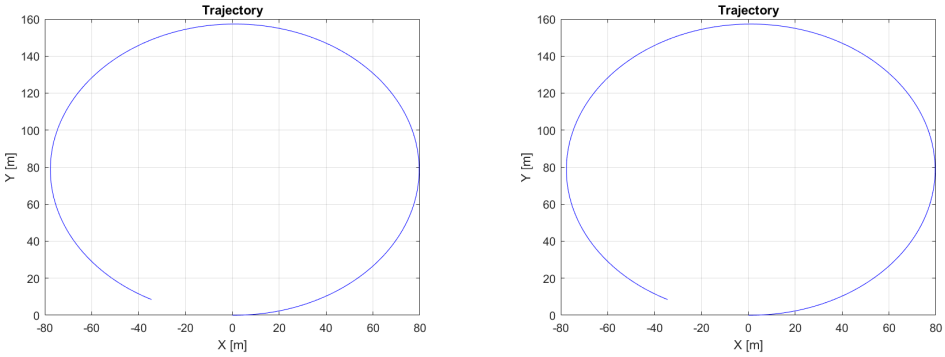

(a) Linear Model (b) Brush Model

A second test was concluded with a larger steering wheel angle of $\delta_{sw} = 180$. Both model still describe a circle, but the brush model describes a significantly larger radius ($20m$ against $17m$). It can be explained by the saturation of the tire at larger slip angles. The respective trajectories are represented figure 24.

Figure 24: Trajectory for $\delta_{sw} = 180$

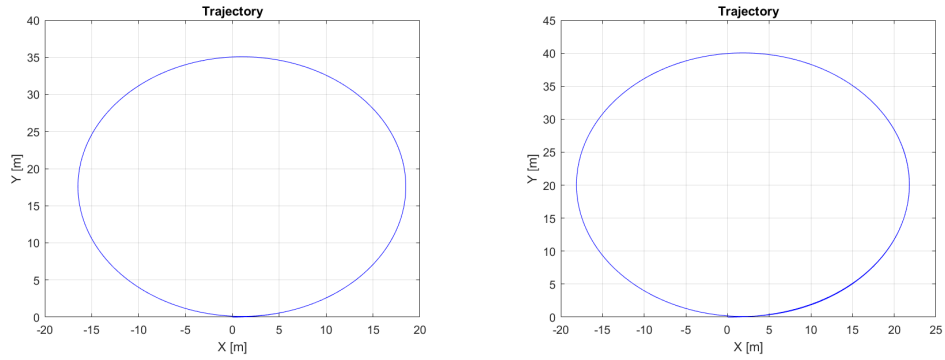

(a) Linear Model (b) Brush Model

4 Model Validation

4.1 Measurements on real conditions

To compare our different models, measurements were made on the real car in different conditions. The testing was performed at Lunda airport. Several sensors were installed on the car to measure in real time all the required parameters. An IMU measures the car position, velocity, acceleration, angular velocity in every direction. All the driver inputs are also being measured, such as the steering angle.

Four different scenarios were tested at different speeds :

- **step steer**. The drive steers instantly from a neutral position of the steering wheel to approximately 90°. It was tested at 50 and 70km/h.
- **ramp steer**. The driver steers progressively from a neutral position to 90°. This scenario was tested at 65km/h.
- **double lane change**. This scenario simulates a sudden change in lane, and then coming back. This scenario was tested at 50, 60,70,80 and 90km/h.
- **slalom**. The driver would slalom around evenly spaced cones. This scenario was tested at 50, 60,70,80 and 90km/h.

All this scenario provides a complete set of data to test out different models.

4.2 Optimization of tyre parameters

All of the tyre models require some parameters. However, this parameters are difficult to measure, and are not provided by the manufacturer. Therefore, to choose accurately the tyre parameter, the MATLAB function **fmincon** was used to minimize the root-mean-square errors between the measured lateral acceleration from testing and the model. Minimizing the root-mean-square error of the yaw rate is also possible and give similar results. The parameters to optimize are the cornering stiffness for the linear model, and the cornering stiffness and the friction coefficient for the brush model. After some early optimization, we notice that the optimized cornering stiffness are similar in both the brush and linear model. Therefore, a first optimization was done with the linear model to compute the cornering stiffness, and then the friction coefficient was optimized.

This process was done on all testing data, and the results are described in table 2. The mean cornering stiffness are $C_{12} = 99kN/rad$ (std of $18kN/rad$), $C_{34} = 90kN/rad$ (std of $20kN/rad$) and the mean friction coefficient is $\mu = 1.26$ (std of 0.3). These values differ depending on the dataset chosen, due to numerical issue and low sensibility of some parameters to the error (especially for the friction coefficient). These values will be used for the model validation.

Scenario	Speed (km/h)	C_{12} (kN/rad)	C_{34} (kN/rad)	μ
Step Steer	50	94	91	1.8
Step Steer	70	104	108	1.5
Ramp Steer	65	148	47	1.3
DLC	50	110	103	1.5
DLC	60	108	93	1.2
DLC	70	90	85	1.9
DLC	80	75	85	1.3
DLC	90	108	135	1
Slalom	50	106	79	0.9
Slalom	60	85	75	1.2
Slalom	70	101	97	0.5
Slalom	80	90	93	1.05
Slalom	90	76	86	1.32

Table 2: Parameter optimization result using **fmincon**

A comparison was made between the Brush model and the linear model. The results are displayed figure 25 for the slalom scenario at 90km/h. No major differences were noticed between the linear and Brush model. Even at very high speed, the tyre slip angles doesn't leave the linear regime. Similar results were achieved with the other scenarios. Therefore in the remaining of the study only the Brush model will be used.

Figure 25: Comparison between the linear and brush model

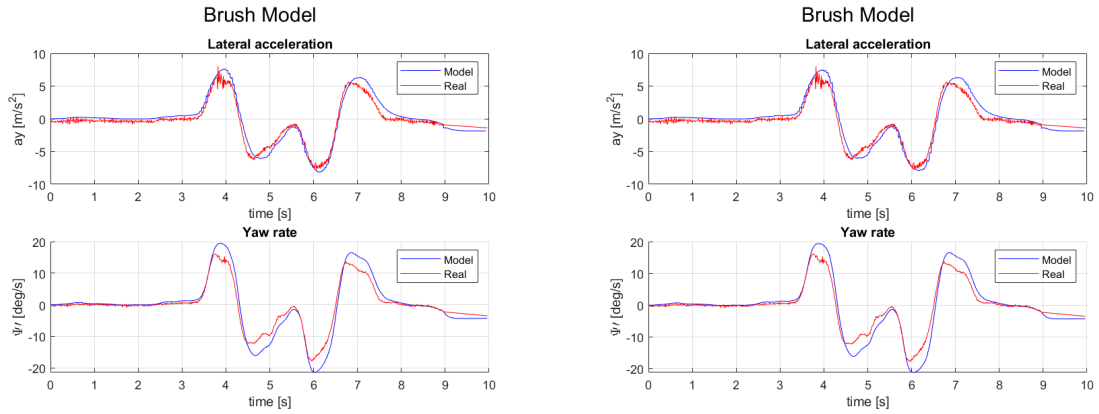

(a) Linear Model

(b) Brush Model

4.3 Validation and comparison

A comparison between the testing data and the ADAMS and matlab models has been made for different scenarios. The results are shown figure 26.

Figure 26: Comparison between matlab, ADAMS and testing data

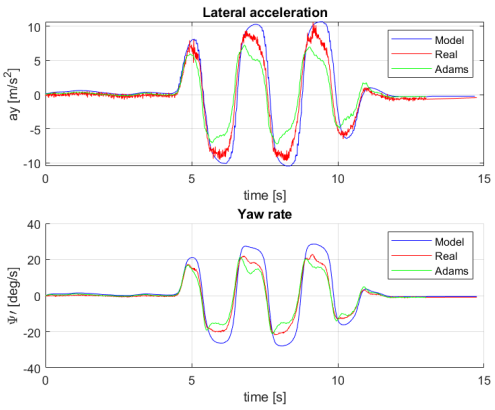

(a) Slalom, 90km/h

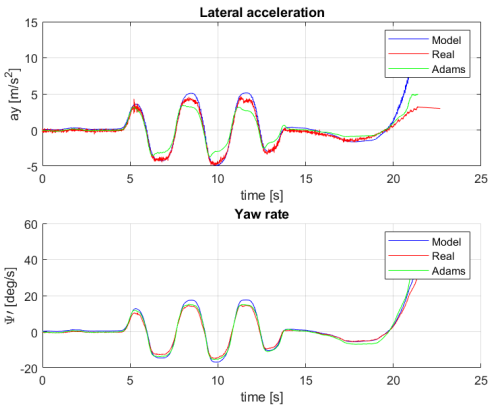

(b) Slalom, 60km/h

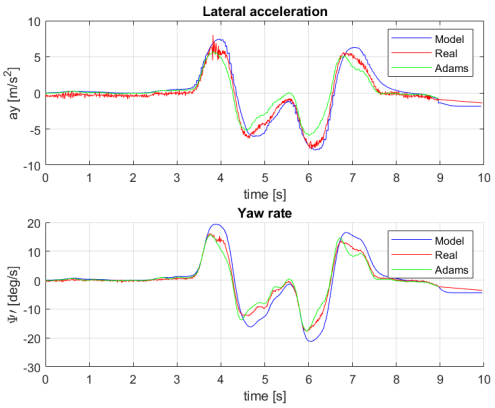

(c) Double lane change, 90km/h

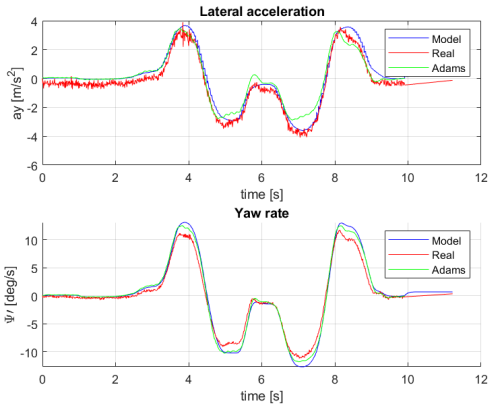

(d) Double lane change, 60km/h

We can see that both matlab and ADAMS model follow the testing data accurately. Therefore, both models are validated. However, the Matlab model is closer to the measured value in most of the scenarios. Furthermore, both models struggle to follow the measurements on high speed maneuvers like the double lane change and slalom at 90km/h, and both models are more precise on the low speeds ones.

5 Parameter study

After validating the model by comparing Adams simulations with the bicycle model and data from the VBOX, a parameter study was conducted in order to deepen or confirm our understanding of some Vehicle Dynamics parameters. First, the total mass of the vehicle was varied, and a step steer maneuver to the right at 80 kmph was implemented to assess the effect of that change. Secondly, a slalom at 80 kmph was used to assess the change of spring stiffness, toe angle, COG height and longitudinal position.

5.1 Parameter study of the mass

The mass of the vehicle was changed by modifying the mass of the chassis. Initially, the mass of the chassis was $m_0 = 1822$ kg, then it was decreased by 20% to $m_1 = 1456$ kg, then by 10% to $m_2 = 1638$ kg, finally it was increased to $m_3 = 2002$ kg. The results are given below for the lateral acceleration, the yaw rate and the vertical load on the front right wheel.

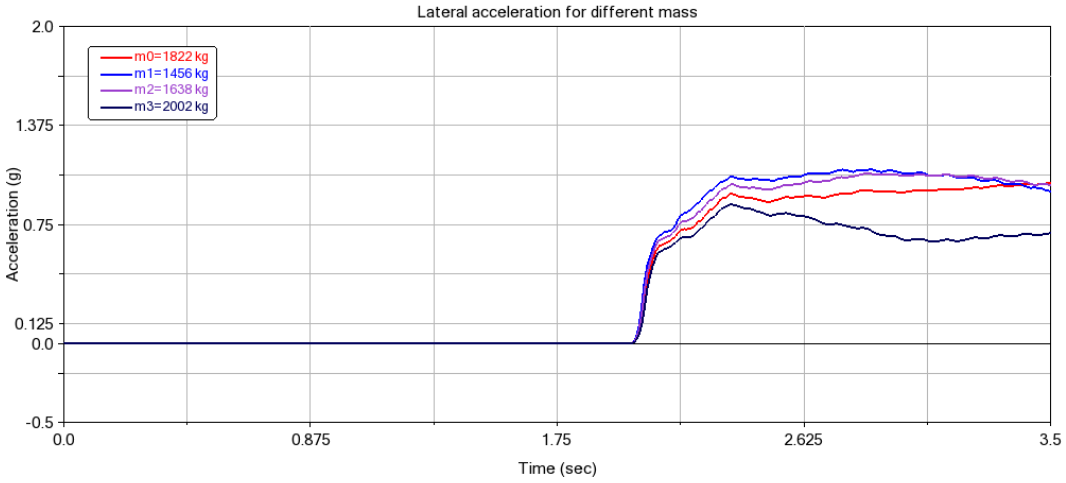

Figure 27: Lateral acceleration a_y for different mass

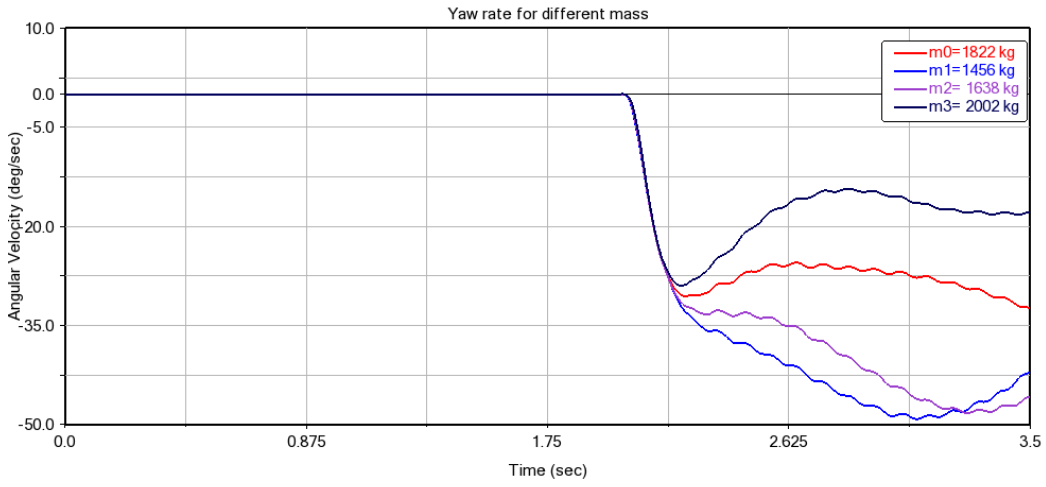

Figure 28: Yaw rate $\dot{\psi}$ for different mass

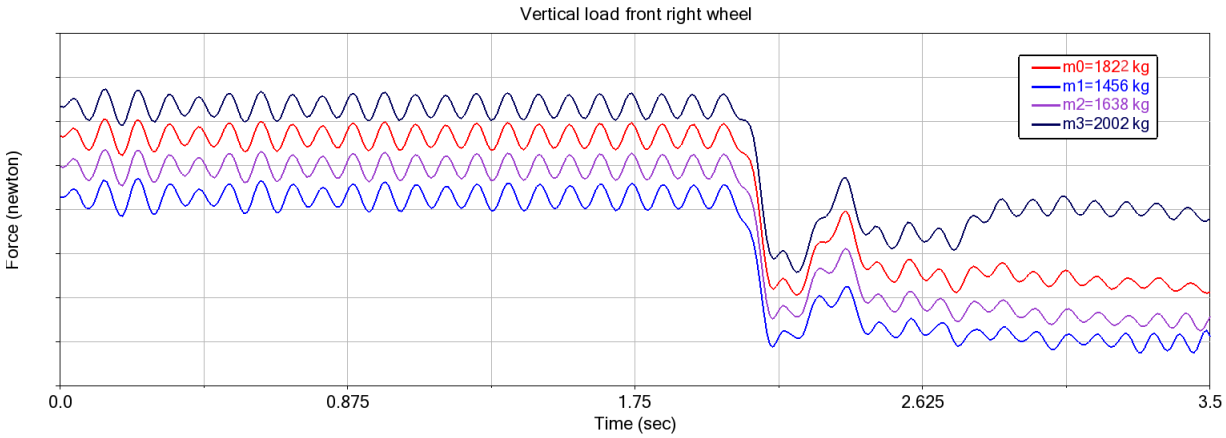

Figure 29: Vertical load front right wheel $F_{z_{fr}}$

First and foremost, some intuitive results are obtained: the higher the mass, the less lateral acceleration is produced (more difficult to steer...), The lower the mass the higher the yaw rate (negative on the figure), as the vehicle moves more easily. Finally, the steering being to the right the load transfer can be seen from the right wheel to the left one (sudden gap at 2 s) and the load is globally higher for a heavier vehicle which was expected.

5.2 COG longitudinal position analysis

During driving conditions, the load distribution could change due to the addition of passengers or luggage to the vehicle or due to the refilling of fuel. In this scenario, it has been analyzed what happens if the center of gravity is moved towards the rear of the vehicle. The parameter λ, defined as the ratio between the distance of the COG with respect to the front axle and the wheelbase ($\lambda = \frac{l_F}{l}$) is increased of the 20%from $\lambda = 0.43$ to $\lambda = 0.55$:

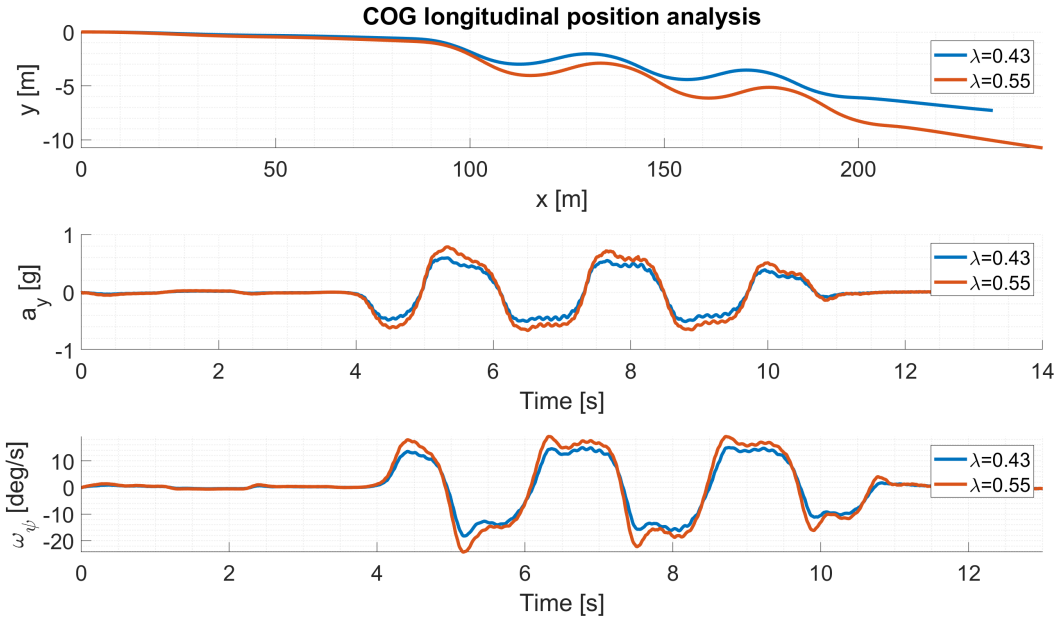

Figure 30: COG longitudinal position analysis

Looking at the trajectory, it is evident how the vehicle is more responsive when steering, presenting higher lateral acceleration and yaw rate. Thus, moving the COG more towards the back improved the overall vehicle agility.

5.3 COG height analysis

Another test undertaken with the COG is to put it more high, as it could be the case of a car with a certain load installed on the roof. The standard COG height of $h_g = 626.3mm$ has been increased by the the 20%, reaching the value $h_g = 751.5mm$:

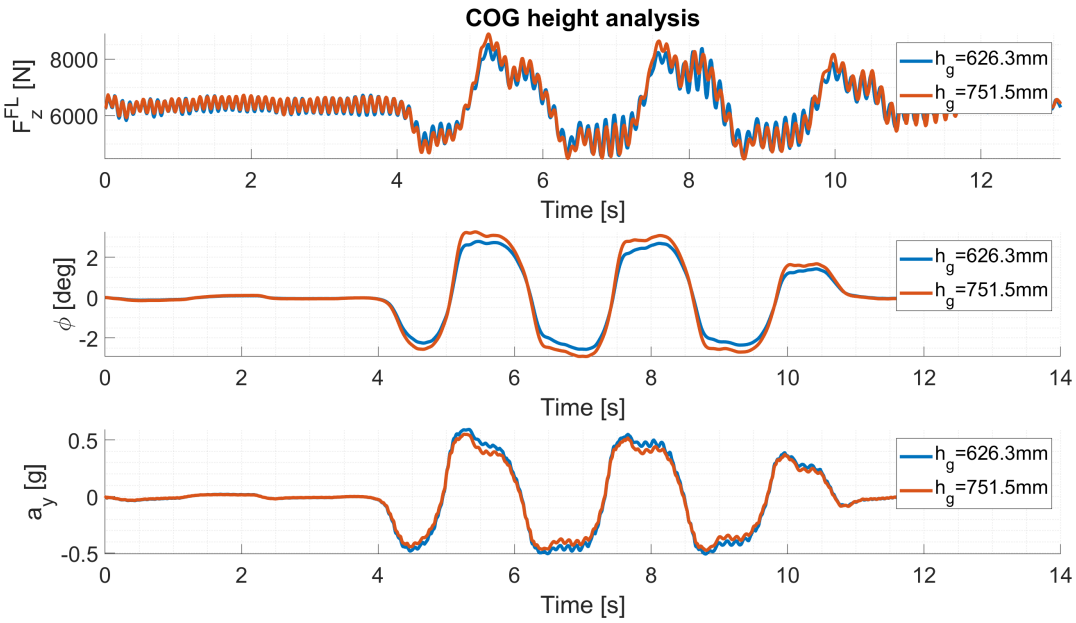

Figure 31: COG height analysis

As expected, the load transfer increases due to the higher inertia force acting on the vehicle, and so does the roll angle.
The lateral acceleration trend is lower, showing that the vehicle agility is more poor in this case.

5.4 Spring stiffness analysis

Another important parameter impacting the vehicle handling performance is the spring stiffness.

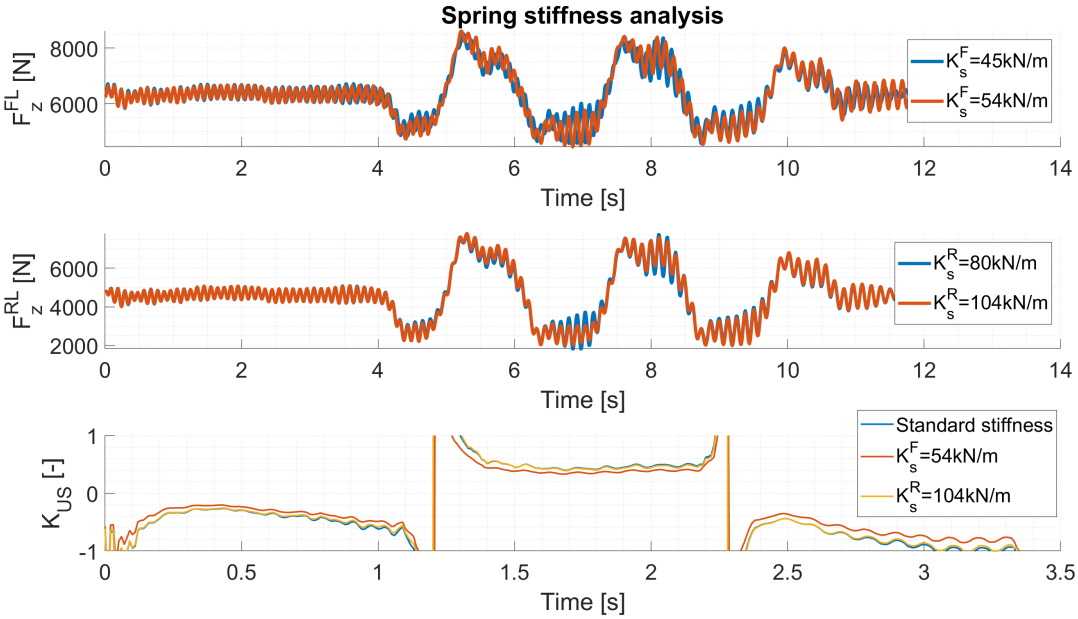

Figure 32: Spring stiffness analysis

Neglecting the effect of the lateral force on the moment equilibrium at the axle level, it is possible to find a relation between the axle rolling stiffness and the vertical force:

$$C \cdot \phi = F_z \cdot t_w \tag{8}$$

Knowing that the axle rolling stiffness is directly proportional to the spring stiffness, it is expected that increasing the spring stiffness, the vertical force transfer is increased as well, considering fixed the lateral inertia force, and so the roll angle.
The results from the simulations prove this expectation. When reading the results of the vertical forces, it must be taken into account that they are relative to only one side of the vehicle, so the load is higher if the tire is the outer one, while it is lower when the tire is the inner one.
Another undertaken analysis concerns the understeering coefficient, computed as:

$$K_{us} = \frac{\alpha_{34} - \alpha_{12}}{a_y} \tag{9}$$

When the front spring stiffness value is increased, it is expected that the vehicle is more understeering (higher K_{us}), due to the cornering stiffness saturation of the front axle caused by the higher vertical load transfer.
Instead, when the rear spring stiffness value is increased, a more oversteering behavior is expected (lower K_{us}).

5.5 Toe analysis

The last parameter to be analyzed is the toe angle. In this case, the toe angle has been separately increased at the front and at the rear to analyze its influence on the car behavior. On both axles, it has been increased from $\phi = 0.1°$ to $\phi = 0.5°$:

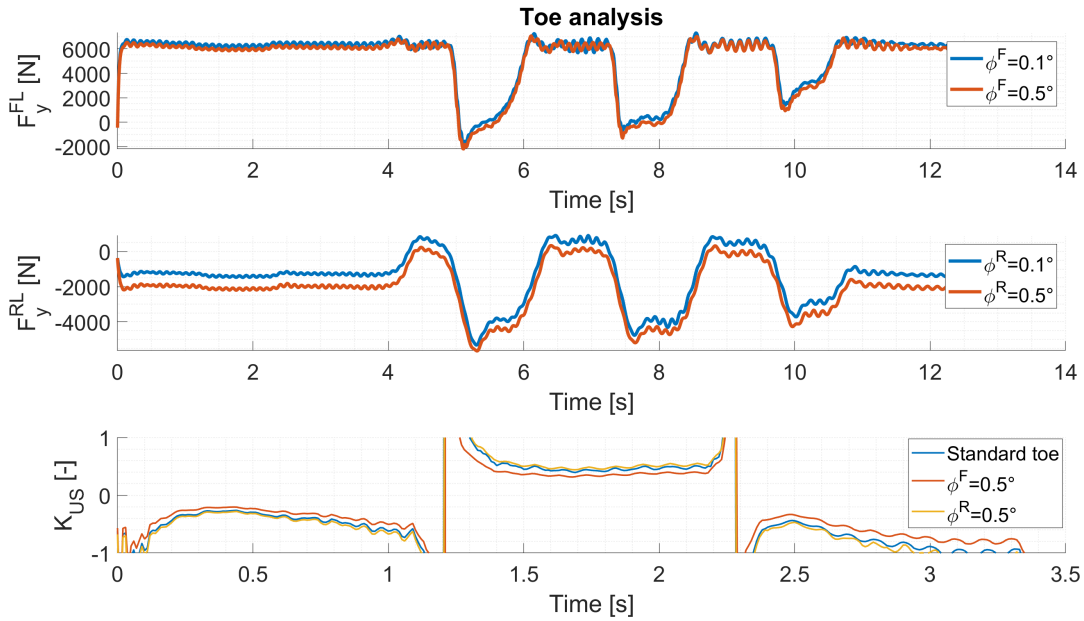

Figure 33: Toe analysis

When increasing the toe angle, it is expected that, when cornering and considering the standard case as reference, the outer tire is steered less, while the inner tire is steered more. Taking this into account, it is expected that the outer tire generates less lateral force, while the inner tire generates a higher lateral force. This expectation is confirmed when looking at the retrieved results.
As in the previous case, the understeering coefficient trend is computed, showing how the vehicle stability trend changes, when varying the toe angles on the two axles.

6 Sources of error

Many sources of error can be identified in this project. Firstly, as accurate as the Adams model may be, the geometries used are approximations of the real vehicle's components. Furthermore, most of the parameters were guessed (cornering stiffnesses, arb stiffness, Inertias...). Besides, for the Matlab part, the bicycle model remains a 2D approximation of the vehicle's motion and can show limitations. Finally, as far as the measurements go, there was no reference from the manufacturer to confirm the accuracy of the data, and the measurements themselves were conducted only once per maneuver (per group). Taking the measurements more than once and studying them statistically could improve the reliability of the results.

7 Conclusion

To conclude this report, this project was an opportunity to improve our knowledge and understanding of vehicle dynamics with a hands-on experience. The lack of familiarity with Adams made the beginning of the project challenging and pushed us to utilize our problem solving skills. The main achievements were the successful modeling of the suspensions, the steering and the correct use of an operational full vehicle assembly to compare with the measurements that were taken at Lunda. Analytical models were used along the journey and a Matlab model was coded using the brush model, which gave satisfactory results. Finally, the parameter study was insightful as it shed light on key dynamic behaviors for a vehicle.